Biases in hand perception are driven by somatosensory computations, not a distorted hand model

Valeria C. Peviani, Luke E. Miller*, W. Pieter Medendorp*

Donders Institute for Cognition and Behavior, Radboud University, Nijmegen, The Netherlands

**Equal contribution*

Corresponding author

Valeria C. Peviani, valeria.peviani@donders.ru.nl

Summary

To sense and interact with objects in the environment, we effortlessly configure our fingertips at desired locations. It is therefore reasonable to assume the underlying control mechanisms rely on accurate knowledge about the structure and spatial dimensions of our hand and fingers. This intuition, however, is challenged by years of research showing drastic biases in the perception of finger geometry, e.g.,[1–5]. This perceptual bias has been taken as evidence that the brain's internal representation of the body's geometry is distorted,[6] leading to an apparent paradox with the skillfulness of our actions.[7] Here, we propose an alternative explanation of the biases in hand perception—They are the result of the Bayesian integration of noisy, but unbiased somatosensory signals about finger geometry and posture. To address this hypothesis, we combined Bayesian reverse-engineering with behavioral experimentation on joint and fingertip localization of the index finger. We modelled the Bayesian integration either in sensory or in space-based coordinates, showing that the latter model variant led to biases in finger perception despite *accurate* representations of finger length. Behavioral measures of joint and fingertip localization responses showed similar biases, which were well-fitted by the space-based but not the sensory-based model variant. Our results suggest that perceptual distortions of finger geometry do not reflect a distorted hand model but originate from near-optimal Bayesian inference on somatosensory signals. These findings demand a reinterpretation of previous work on hand model distortions.

Keywords

Somatic perception; body representation; finger kinematics; Bayesian brain; computational modeling; coordinate transformation; spatial perception; postural priors

RESULTS

One of the most surprising neuroscientific findings over the last two decades is that the spatial perception of our body appears to be highly distorted, even for body parts that are required for fine-grained motor control, such as the hand and fingers.[1] A widespread assumption is that the perceptual biases measured in these experiments *directly* reflect a distorted internal representation of body geometry. Taking this inference at face value for the hand leads to what has been termed the 'hand paradox':[7] How are distorted hand representations compatible with the observed skillfulness of our manual actions?

Here, we address this paradox. In contrast to the standard interpretation, we propose that the observed perceptual biases do not reflect a distorted hand model; rather, these biases arise from probabilistic computations that perform near-optimal Bayesian inference on somatosensory signals. We took a two-pronged approach to investigate whether this optimal probabilistic processing can explain the perceptual biases observed in a finger mapping task: First, we formalized and modelled the optimal computations that may underlie the transformation of somatosensory signals about finger configuration into its spatial dimensions (**Figure 1**). This allowed us to obtain quantitative predictions pertaining to spatial errors in finger mapping. We then tested these predictions using a novel VR-based finger mapping task, combined with fitting our computational models to the observed responses (**Figure 2**).

A Bayesian model of finger perception

We developed a model of how somatosensory signals about finger geometry (i.e., joint angles, phalanx lengths) are transformed into a percept of where the finger is in space. To do so, we conceptualized the geometry of the finger as a kinematic chain, where each finger segment is linked with the previous segment through the interphalangeal joints (**Figure 1A**). In the periphery, somatosensory signals encode the length L of each phalanx and the angle θ of each of the three interphalangeal joints. As illustrated in **Figure 1A**, this information allows to derive the spatial positions of the joints and the fingertip, following:

$$\boldsymbol{l}_n = (x_n, y_n) = \sum_{i=1}^{n} L_i \,(\cos\varphi_i\,, \sin\varphi_i) \quad \text{with } \varphi_n = \sum_{i=1}^{n} \theta_i \qquad (1)$$

Where $\boldsymbol{l}_n$ is the two-dimensional location of the proximal or distal interphalangeal joint or the fingertip. However, this formulation is not sufficient to specify the underlying computations used by the nervous system. The brain does not represent the angles, lengths, and locations as individual point estimates but rather as probability distributions.[8] This is because the activity within the nervous system is intrinsically noisy, from transduction of signals to network interactions.[9] To deal with this uncertainty, the brain must rely on probabilistic processing, as formalized by Bayesian decision theory.[10,11] For

perception, the Bayesian framework states that the observer forms a belief (the posterior) about the most probable state of the body and the world. This is done by integrating noisy sensory signals with prior beliefs, following Bayes' rule. The final posterior corresponds to the weighted average of the likelihood and prior, with the weights equating their respective precisions. Importantly for our purposes, this computation yields an increase in perceptual precision at the expense of a bias in perception.

We therefore re-formalized the geometric model of the finger in Eq. (1) in probabilistic terms (**Figure 1B**). The spatial percept of the finger (posterior) is constructed by integrating the somatosensory measurements (likelihood) with prior information about its most probable configuration (prior), possibly inferred from an accumulated history of the finger's previous configurations.[11] Since the size of our fingers remain stable in the short-term, it is reasonable to assume that prior information on segment length L is accurate, i.e., centered on true values.

For each $\boldsymbol{l}_n$, we specify the likelihood and the prior as vectors, with their respective means ($\boldsymbol{\mu}_{lik}$and $\boldsymbol{\mu}_{pr}$) and diagonal variance-covariance matrices (Σ_{lik} and Σ_{pr}). Following Bayes' rule, the posterior is obtained from the product of the likelihood and prior. In matrix-form, this is formalized as follows:

$$\boldsymbol{\mu}_{pos} = \left(\Sigma_{pr}^{-1} + \Sigma_{lik}^{-1}\right)^{-1}\left(\Sigma_{pr}^{-1}\boldsymbol{\mu}_{pr} + \Sigma_{lik}^{-1}\boldsymbol{\mu}_{lik}\right) \quad (2)$$

$$\Sigma_{pos}^{-1} = \Sigma_{pr}^{-1} + \Sigma_{lik}^{-1} \quad (3)$$

where Eq. (2) is the computation of the posterior mean ($\boldsymbol{\mu}_{pos}$) and Eq. (3) is the computation of the posterior variance-covariance matrix (Σ_{pos}), assuming that the Bayesian integration is performed optimally.

We consider two distinct model variants that formalize how the sensory-to-space transformation (Eq. 1) and Bayesian Integration (Eqns. 2 and 3) are implemented in the somatosensory processing hierarchy (**Figure 1C**).

In **model variant 1** (**Figure 1B,** top; **Figure 1C**, blue), Bayesian integration occurs *before* the sensory-to-space transformation. That is, the likelihood and the prior in Eqns. (2-3) are defined in sensory coordinates, representing the involved joint angles ($\theta_1, \dots, \theta_n$) and phalanx lengths ($L_1, \dots, L_n$). The likelihood is specified as a Gaussian distribution with mean $\boldsymbol{\mu}_{lik}$ and diagonal variance-covariance matrix Σ_{lik}, where all off-diagonal are zero (i.e., assuming uncorrelated signals). The prior is likewise specified as Gaussian with mean $\boldsymbol{\mu}_{pr}$ and variance-covariance matrix Σ_{pr}; however, unlike the likelihood, we did allow covariance between subsequent joints. Following Bayesian integration (Eqns. 2-3), the posteriors of the joint angles and segment lengths are then transformed into space-based posteriors of the joints of fingertip, involving the Jacobian transformation as derived from Eq. (1), see **Supplemental Materials**.

In **model variant 2** (**Figure 1B,** bottom; **Figure 1C**, green), Bayesian integration occurs *after* the sensory-to-space transformation. In this variant, the sensory likelihood distributions are first transformed into space-based likelihoods of joint and fingertip position (i.e., $\boldsymbol{\mu}_{lik}$ and Σ_{lik} specified in Cartesian coordinates). These are then integrated with the transformed spatial prior ($\boldsymbol{\mu}_{pr}$, with Σ_{pr}) as in Eqns. (2-3) to obtain the space-based posterior of the joints and fingertip positions.

Near-optimal computations predict perceptual biases in finger perception

We next identified the differences in the quantitative predictions made by each model variant. Our goal here was two-fold. First, we aimed to distinguish specific testable predictions made by each model. Second, and relatedly, we aimed to pinpoint when—if ever—these computations would lead to distorted perception of joint and fingertip locations. To do so, we simulated the above computations across a variety of model parameters and finger postures.

Figure 1C illustrates the computational outcomes of each model in a Cartesian reference frame. In both model variants the posterior distribution is biased relative to the actual joint position. Crucially, only in variant 2 do these biases affect the perceived geometry of the finger. Interestingly, these finger length distortions were a ubiquitous consequence of Bayesian integration occurring after the sensory-to-space transformation. This is despite the fact that the underlying likelihood and prior accurately reflected finger size.

Simulations with model variant 2 further revealed that the magnitude of finger length misestimation varied as a function of posture. **Figure 1D** illustrates how the percentage of total finger length misestimation varies as a function of the statistical distance between the spatial likelihood and the spatial prior (**Figure S1, SM**). As this distance increases, only model variant 2 predicts the emergence of length misestimation. Hence, the posture-dependence of the inferred finger length is the key difference between the predictions of the two model variants. Crucially, this posture-dependent misestimation would not be predicted if perceptual biases were only a consequence of distorted representation of finger length.

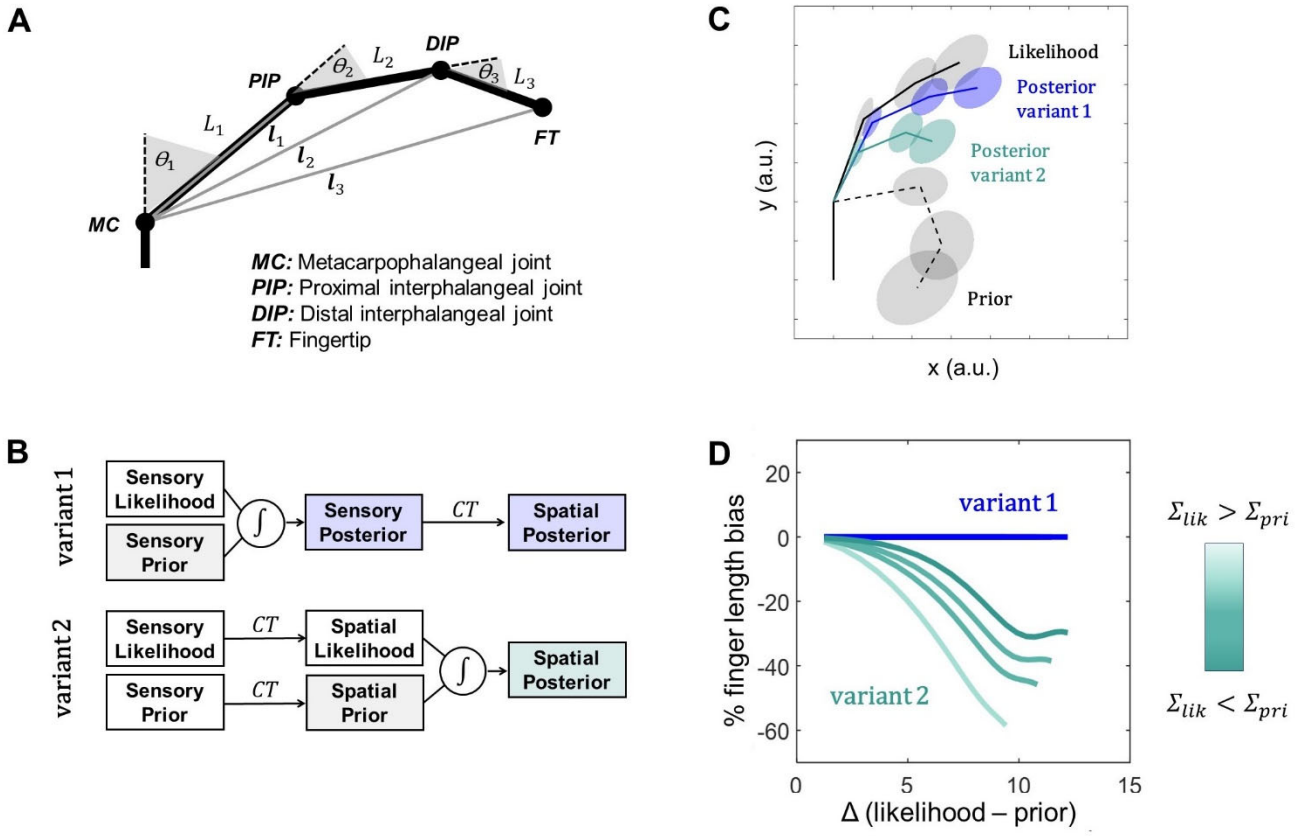

Figure 1. A Bayesian model of finger perception. A. Geometric model of the finger as a kinematic chain. The chain allows one-axis rotations. The three segments (L_1, L_2, L_3) are interconnected by three joints $(\theta_1, \theta_2, \theta_3)$, corresponding to the MC, PIP and DIP. The spatial positions of PIP, DIP and FT are defined as 2D vectors l_1, l_2, l_3, each with respect to MC. **B.** Schematic representation of the Bayesian model of finger perception. Variant 1: Bayesian integration ($\int$) occurs before the sensory-to-space transformation (*CT*). Variant 2: Bayesian integration occurs after the sensory-to-space transformation. **C.** Model predictions: both variants plotted in Cartesian coordinates (likelihood, solid gray; prior, dashed gray; posterior variant 1, blue, posterior variant 2, green). Variant 1 predicts biases in joint angle, not phalanx length. Variant 2 predicts biases in both, as if the overall length of the finger is underestimated. **D.** Finger length bias plotted as a function of the distance between likelihood and prior. Variant 2 predicts that this bias increases with this distance (see also Figure S1,SM).

Probing model predictions in a novel VR finger-mapping paradigm

To test model's predictions, we designed a VR task that measures position estimates of unseen index finger joints and fingertip at varying finger postures. Participants (N=20) used a hand-held virtual pointer to indicate the felt position of each of these (**Figure 1A**). To ensure stable but varying finger configurations throughout the task, participants firmly held postural shapes of variable sizes. In all, the experiment consisted of a total of 600 position estimates, divided into separate blocks of 100 trials, each related to one of six finger configurations (**Figure 2,** and **SM**). We used a reverse-engineering approach to identify which model (**Figure 1B**) provided the best fit to each participant's trial-wise position estimates.

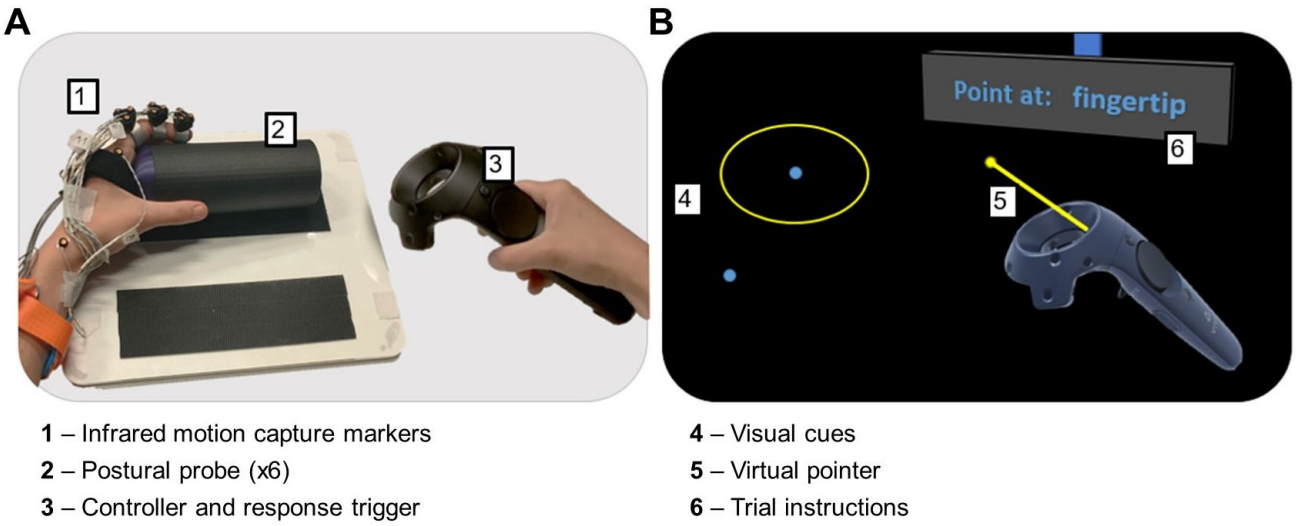

Figure 2. Experimental task and stimuli. A. Participants wore a VR headset, while their head was supported by a chin rest. Different finger configurations were probed by holding differently sized objects (cylindric volumes diameter 20, 30, 40 cm) with a power grip. The position of left wrist, left index MC, PIP, DIP and FT, were recorded using infrared motion tracking. **B.** The VR environment presented a dark 3D space in which experimental instructions were displayed on a screen. Blue spheres (diameter 5 mm) indicated the physical locations of participants' left wrist and MC. Information on total index finger length was conveyed by rendering a yellow circle centered on MC. Using a hand-held controller, participants had to put the tip of a virtual pointer on the perceived locations of their PIP, DIP or FT (600 trials across 6 postures).

In all participants, the results of our experiment matched the predictions from model variant 2. **Figure 3** illustrates the data of four representative participants, showing that the perceived location of finger joints and tip differed from their actual locations (**Figure 3A**, actual posture in black, responses in gray; **Figure S2, SM**). This finding is consistent with the notion that Bayesian priors bias perception. Crucially, the observed biases took on two patterns: First, the perceived angle of the finger deviated from the actual angle, suggesting the role of a prior over joint angles in perception; Second, the perceived finger length differed from the actual finger length, suggesting that perceptual biases may arise

from Bayesian computations occurring in Cartesian space, after the sensory signals are transformed in spatial coordinates.

Model fitting (see **SM**) confirmed these initial observations. The fits for each model variant to the data of representative participants can be seen in **Figure 3A**. For all participants, integration after the sensory-to-space transformation (model variant 2) best explained the behavioral observations, with consistently lower BICs compared to model variant 1 (**Figure 3B**). Unlike model variant 1 and the hypothesis of distorted representations, model variant 2 predicts posture-dependent finger length misestimation biases. These predictions were correlated with the observed behavior (Pearson's $r = 0.46$, $p<.001$): the larger the discrepancy between the likelihood and prior, the greater the magnitude of finger length underestimation (**Figure 3C**). Follow-up data inspection ruled out the possibility that underestimation was due to the nature of our task, which could have led to truncation in position estimates made by participants (**Figure S3**, **SM**).

These findings bring to light two key features of the computation used by the brain to transform somatosensory inputs into the perception of the body in space. First, estimating the finger's position in space results from optimal integration of transformed sensory inputs with stored priors. Second, optimal integration between sensory and stored signals occurs between estimates of finger posture in a space-based, Cartesian reference frame. Together, the features of this computation lead to the consistently observed distortions in finger length perception. We discuss the implications in the following section.

DISCUSSION

Previous empirical observations can be taken to suggest that postural priors influence proprioceptive and tactile processing. For example, during temporary limb anesthesia, limb perception systematically changes towards a semi-flexed posture.[12,13] Placing the fingers or upper limbs in unusual postures leads to less efficient tactile processing.[14–20] Going beyond these observations, our work is the first to quantitatively define and empirically verify the influence of a postural prior on the perception of the body in space. More crucially, our findings constrain the nature of this prior, suggesting that it is encoded in spatial (Cartesian) and not sensory coordinates (**Figure 1C**). A consequence of this computational scheme is that Bayesian integration occurs only after sensory signals (i.e., likelihoods) are themselves transformed into a spatial estimate of finger location.

There are important functional reasons why the brain would perform somatosensory inference in Cartesian spatial coordinates. For example, doing so would aid in multisensory integration (e.g., vision and proprioception), where sensory signals must be transformed from their native sensor-based coordinates into a shared spatial frame of reference. Bayesian multisensory integration is indeed a basis

for body perception,[21] the bodily self,[22–24] and sensorimotor control.[25] We propose that the model of the present study reflects the first step in these processes, transforming signals into a reference frame that could be shared amongst different sensory modalities, including the construction of peripersonal space.[26,27] Doing so allows posterior parietal areas to 'project the body into the world'.[28]

A major area of inquiry over the last decade has been the origin of distortions in hand perception. According to a recent conceptual model of body representation,[29] postural priors are not sufficient to explain distortions in metric hand perception. Instead, perceptual distortions are the direct consequence of integrating somatosensory inputs with a distorted body representation (i.e., a body model). Both our simulations and empirical findings stand in contrast to this claim. Our results instead suggest that distortions in finger length perception are due to the nature of the computation; Specifically, spatial finger perception is the result of Bayesian integration between a spatial likelihood and prior (i.e., model variant 2) that each *accurately* encode finger length. One unique piece of evidence in favor of the present proposal is the posture-dependence on finger length misestimation (**Figure 3** and **Figure S1, SM**). These findings reconcile the notion of perceptual biases in finger perception with optimal sensorimotor processing, as all signals used for control would be unbiased.

Recent neurophysiological studies suggest that the computations identified in our study occur as early as primary somatosensory cortex (S1). Postural signals are ubiquitous throughout primary somatosensory cortex.[30] Indeed, multimodal neurons in Area 2 are known to encode the posture of the forelimb in Cartesian coordinates. Crucially, two recent human fMRI studies found that multivariate patterns of neural activity in S1 significantly correlate with the spatial features of the hand and even more so with the spatial features of biased hand perception.[31,32] In this context, these studies suggest that the Bayesian computations that produce geometric finger distortions occur in early somatosensory cortical processing. We hypothesize that the integration of the spatial likelihood and prior is implemented in S1, perhaps through biases in tuning curve distributions[33] and/or neural population dynamics.[34]

We conclude that perceptual biases are driven by near-optimal somatosensory computations, not a distorted hand model. This new perspective on the nature of somatosensory computations *dissolves* the 'hand paradox'. That is, regardless of the relationship between hand perception and manual actions,[4,35] the processes subserving each rely on likelihoods and priors that accurately reflect hand geometry. Our proposed resolution to the hand paradox opens a new window on the understanding of body representations.

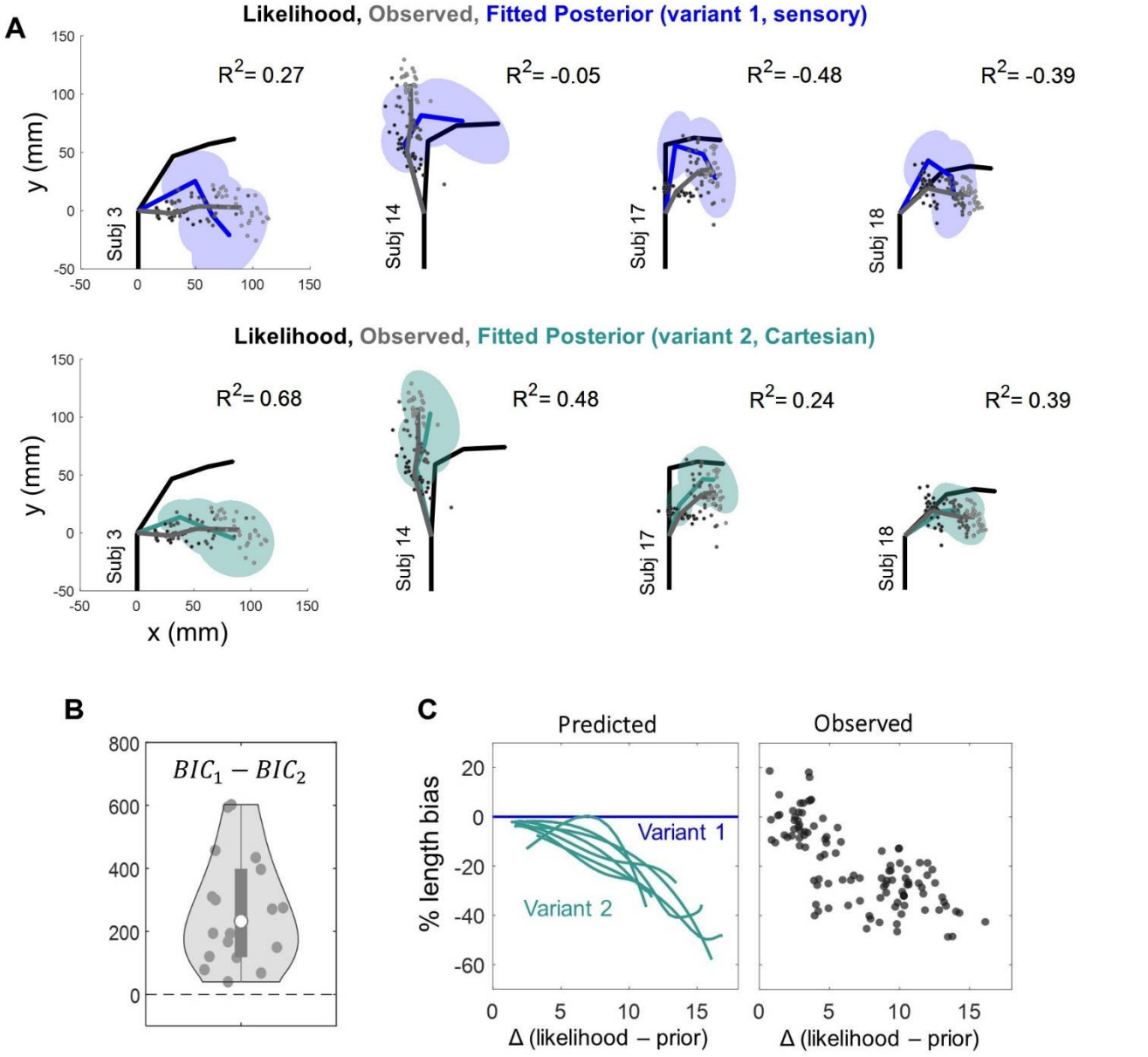

Figure 3. Near-optimal computations underlie biases in finger perception. A. Data of four representative participants for one of six finger configurations (in black). Localization responses of PIP, DIP and FT are represented as gray dots and their means are connected by gray lines. Model fits are shown as the mean of the posterior for these locations (variant 1, in blue; variant 2, in green). **B.** Model variant 2 outperformed variant 1 for all participants. The mean BICs were 8410 ± 442 for variant 1 and 8143 ± 499 for variant 2, with significantly lower BIC for variant 2 ($t(17) = 6.5$, $p < .001$, CIs: 179, 351). Model variant 2 explained on average 35% of the variance; variant 1 performed worse than the null model. **C.** Bayesian integration predicts posture-dependent biases in finger perception. We simulated spatial posteriors based on best-fit model variants of each subject for several finger configurations ranging from fully extended to flexed. Based on these posteriors, we plot the bias in finger length as a function of the statistical distance between likelihood and prior. Predictions are represented as lines in the left panel, observations are represented as solid dots in the right panel.

Acknowledgements

This research is funded by the Radboud Excellence Initiative grant awarded to V.C.P.

We extend our gratitude to the Sensorimotor Lab members for the numerous scientific discussions, and the Technical Support Group of DCC for their invaluable assistance and expertise.

Author contributions

V.C.P., L.E.C.M., W.P.M., Conceptualization; Methodology

V.C.P., Funding Acquisition, Investigation, Writing – Original Draft

L.E.C.M., W.P.M., Supervision, Writing – Review & Editing, Resources

Declaration of interests

The authors declare no competing interests.

References

1. Longo, M.R., and Haggard, P. (2010). An implicit body representation underlying human position sense. Proc Natl Acad Sci U S A *107*, 11727–11732. 10.1073/PNAS.1003483107/SUPPL_FILE/PNAS.201003483SI.PDF.
2. Coelho, L.A., and Gonzalez, C.L. (2018). The visual and haptic contributions to hand perception. Psychol Res *82*, 866–875. 10.1007/s00426-017-0870-x.
3. Saulton, A., Longo, M.R., Wong, H.Y., Bülthoff, H.H., and de la Rosa, S. (2016). The role of visual similarity and memory in body model distortions. Acta Psychol (Amst) *164*, 103–111. 10.1016/j.actpsy.2015.12.013.
4. Peviani, V., and Bottini, G. (2018). The distorted hand metric representation serves both perception and action. Journal of Cognitive Psychology *30*, 880–893. 10.1080/20445911.2018.1538154.
5. Longo, M.R. (2019). Sex differences in perceptual hand maps: A meta-analysis. Acta Psychol (Amst) *196*, 1–10. 10.1016/j.actpsy.2019.03.002.
6. Longo, M.R. (2022). Distortion of mental body representations. Preprint at Elsevier Ltd, 10.1016/j.tics.2021.11.005 10.1016/j.tics.2021.11.005.
7. Bassolino, M., and Becchio, C. (2023). The 'hand paradox': distorted representations guide optimal actions. Trends Cogn Sci *27*, 7–8. 10.1016/j.tics.2022.09.010.
8. Miller, L.E., Fabio, C., Azaroual, M., Muret, D., van Beers, R.J., Farn, A., and Pieter Medendorp, W. A neural surveyor to map touch on the body. 10.1073/pnas.2102233118/-/DCSupplemental.
9. Faisal, A.A., Selen, L.P.J., and Wolpert, D.M. (2008). Noise in the nervous system. Preprint, 10.1038/nrn2258 10.1038/nrn2258.
10. Ma, W.J., Beck, J.M., Latham, P.E., and Pouget, A. (2006). Bayesian inference with probabilistic population codes. Nat Neurosci *9*, 1432–1438. 10.1038/nn1790.
11. Kording, K.P., Tenenbaum, J.B., and Shadmehr, R. (2007). The dynamics of memory as a consequence of optimal adaptation to a changing body. Nat Neurosci *10*, 779–786. 10.1038/nn1901.
12. Melzack, R., and Bromage, P.R. (1973). Experimental Phantom Limbs.
13. Inui, N., Masumoto, J., Ueda, Y., and Ide, K. (2012). Systematic changes in the perceived posture of the wrist and elbow during formation of a phantom hand and arm. Exp Brain Res *218*, 487–494. 10.1007/s00221-012-3040-9.
14. Yamamoto, S., and Kitazawa, S. (2001). Reversal of subjective temporal order due to arm crossing.
15. de Haan, A.M., Anema, H.A., and Dijkerman, H.C. (2012). Fingers Crossed! An Investigation of Somatotopic Representations Using Spatial Directional Judgements. PLoS One *7*. 10.1371/journal.pone.0045408.
16. Heed, T., Backhaus, J., and Rôder, B. (2012). Integration of Hand and Finger Location in External Spatial Coordinates for Tactile Localization. Journal of Experimental Psychology; Human Perception and Perfonnance *38*, 386–401. 10.l037/a0024059.
17. Azañón, E., Radulova, S., Haggard, P., and Longo, M.R. (2016). Does the crossed-limb deficit affect the uncrossed portions of limbs? J Exp Psychol Hum Percept Perform *42*, 1320–1331. 10.1037/XHP0000206.
18. Romano, D., Marini, F., and Maravita, A. (2017). Standard body-space relationships: Fingers hold spatial information. Cognition *165*, 105–112. 10.1016/j.cognition.2017.05.014.
19. Romano, D., Tamé, L., Amoruso, E., Azañón, E., Maravita, A., and Longo, M.R. (2019). The standard posture of the hand. J Exp Psychol Hum Percept Perform *45*, 1164–1173. 10.1037/XHP0000662.
20. Badde, S., and Heed, T. (2023). The hands' default location guides tactile spatial selectivity. Proc Natl Acad Sci U S A *120*. 10.1073/pnas.2209680120.
21. Clemens, I.A.H., de Vrijer, M., Selen, L.P.J., van Gisbergen, J.A.M., and Medendorp, W.P. (2011). Multisensory processing in spatial orientation: An inverse probabilistic approach. Journal of Neuroscience *31*, 5365–5377. 10.1523/JNEUROSCI.6472-10.2011.
22. Fang, W., Li, J., Qi, G., Li, S., Sigman, M., and Wang, L. (2019). Statistical inference of body representation in the macaque brain. Proc Natl Acad Sci U S A *116*, 20151–20157. 10.1073/pnas.1902334116.

23. Samad, M., Chung, A.J., and Shams, L. (2015). Perception of body ownership is driven by Bayesian sensory inference. PLoS One *10*. 10.1371/journal.pone.0117178.

24. Chancel, M., and Ehrsson, H.H. (2023). Proprioceptive uncertainty promotes the rubber hand illusion. Cortex *165*, 70–85. 10.1016/j.cortex.2023.04.005.

25. Bertoni, T., Mastria, G., Akulenko, N., Perrin, H., Zbinden, B., Bassolino, M., and Serino, A. (2023). The self and the Bayesian brain: Testing probabilistic models of body ownership through a self-localization task. Cortex *167*, 247–272. 10.1016/j.cortex.2023.06.019.

26. Noel, J.P., Pfeiffer, C., Blanke, O., and Serino, A. (2015). Peripersonal space as the space of the bodily self. Cognition *144*, 49–57. 10.1016/j.cognition.2015.07.012.

27. Serino, A. (2019). Peripersonal space (PPS) as a multisensory interface between the individual and the environment, defining the space of the self. Preprint at Elsevier Ltd, 10.1016/j.neubiorev.2019.01.016 10.1016/j.neubiorev.2019.01.016.

28. Medendorp, W.P., and Heed, T. (2019). State estimation in posterior parietal cortex: Distinct poles of environmental and bodily states. Preprint at Elsevier Ltd, 10.1016/j.pneurobio.2019.101691 10.1016/j.pneurobio.2019.101691.

29. Tamè, L., Azañón, E., and Longo, M.R. (2019). A conceptual model of tactile processing across body features of size, shape, side, and spatial location. Preprint at Frontiers Media S.A., 10.3389/fpsyg.2019.00291 10.3389/fpsyg.2019.00291.

30. Kim, S.S., Gomez-Ramirez, M., Thakur, P.H., and Hsiao, S.S. (2015). Multimodal interactions between proprioceptive and cutaneous signals in primary somatosensory cortex. Neuron *86*, 555–566. 10.1016/j.neuron.2015.03.020.

31. Mastria, G., Scaliti, E., Mehring, C., Burdet, E., Becchio, C., Serino, A., and Akselrod, M. (2023). Morphology, Connectivity, and Encoding Features of Tactile and Motor Representations of the Fingers in the Human Precentral and Postcentral Gyrus. Journal of Neuroscience *43*, 1572–1589. 10.1523/JNEUROSCI.1976-21.2022.

32. Tamè, L., Tucciarelli, R., Sadibolova, R., Sereno, M.I., and Longo, M.R. (2021). Reconstructing neural representations of tactile space. Neuroimage *229*. 10.1016/j.neuroimage.2021.117730.

33. Girshick, A.R., Landy, M.S., and Simoncelli, E.P. (2011). Cardinal rules: Visual orientation perception reflects knowledge of environmental statistics. Nat Neurosci *14*, 926–932. 10.1038/nn.2831.

34. Sohn, H., Narain, D., Meirhaeghe, N., and Jazayeri, M. (2019). Bayesian Computation through Cortical Latent Dynamics. Neuron *103*, 934-947.e5. 10.1016/j.neuron.2019.06.012.

35. Peviani, V., Liotta, J., and Bottini, G. (2020). The motor system (partially) deceives body representation biases in absence of visual correcting cues. Acta Psychol (Amst) *203*. 10.1016/j.actpsy.2020.103003.

36. Veale, J.F. (2014). Edinburgh Handedness Inventory - Short Form: A revised version based on confirmatory factor analysis. Laterality *19*, 164–177. 10.1080/1357650X.2013.783045.

37. Hadi, A.S. (1992). Identifying Multiple Outliers in Multivariate Data. Article in Journal of the Royal Statistical Society Series B. 10.2307/2345856.

38. Santello, M., Flanders, M., and Soechting, J.F. (1998). Postural Hand Synergies for Tool Use.

39. Santello, M., Flanders, M., and Soechting, J.F. (2002). Patterns of Hand Motion during Grasping and the Influence of Sensory Guidance.

40. McGuire, L.M.M., and Sabes, P.N. (2009). Sensory transformations and the use of multiple reference frames for reach planning. Nat Neurosci *12*, 1056–1061. 10.1038/nn.2357.

SUPPLEMENTAL MATERIALS

A Bayesian model of finger spatial perception

To model the kinematics of a system such as the finger, it is useful to consider it as a kinematic chain, thereby specifying the relevant degrees of freedom. For simplicity, we assume that the finger only flexes or extends, as realized by a combination of one-axis rotations of the three interphalangeal joints (i.e., metacarpophalangeal joint (MC), proximal interphalangeal joint (PIP) and distal interphalangeal joint (DIP)). If the hand is fixed in space, the locations of PIP, DIP, and fingertip (FT), as probed in the experiment, can be expressed in a 2D Cartesian frame of reference, centered at MC, with the y-axis such that it is aligned with the finger when the finger is fully extended, and the x-axis orthogonal to it (see **Figure 1A**).

We define the rotation angles of MC, DIP and PIP as θ_1, θ_2 and θ_3 and the lengths of the base, middle, and tip phalanges as $L_1, L_2,$ and L_3, respectively. Assuming these variables as noiseless, the spatial, Cartesian location of DIP, PIP and FT, defined as 2D vectors, $\boldsymbol{l}_n = f(\theta_1, \cdots, \theta_n., L_1, \cdots, L_\mathrm{n})$, are geometrically specified as follows:

$$\boldsymbol{l}_n = (x_n, y_n) = \sum_{i=1}^{n} L_i\,(\cos\varphi_i\,, \sin\varphi_i) \quad \text{with } \varphi_n = \sum_{i=1}^{n} \theta_i \tag{1}$$

Because noise is ubiquitous in the nervous system, a neural computation of Eq. (1) relies on noisy sensory inputs of the involved joint angles and phalanx lengths, yielding outcomes that are described not as single points but rather as probability distributions over possible positions, as formalized by Bayes' theorem.

To provide a theoretical framework that explains the observed responses, we designed a probabilistic model of the kinematic chain that assumes optimal Bayesian processing of all potentially relevant signals. For each $\boldsymbol{l}_n$, we specify the likelihood and the prior with means $\boldsymbol{\mu}_{lik}$ and $\boldsymbol{\mu}_{pr}$, respectively, and diagonal covariance matrix Σ_{lik} and Σ_{pri}. Following Bayes' rule, the posterior is obtained from the product of the likelihood and prior. In matrix-form, this is formalized as follows:

$$\boldsymbol{\mu}_{pos} = \left(\Sigma_{pr}^{-1} + \Sigma_{lik}^{-1}\right)^{-1}\left(\Sigma_{pr}^{-1}\boldsymbol{\mu}_{pr} + \Sigma_{lik}^{-1}\boldsymbol{\mu}_{lik}\right) \tag{2}$$

$$\Sigma_{pos}^{-1} = \Sigma_{pr}^{-1} + \Sigma_{lik}^{-1} \tag{3}$$

where Eq. (2) is the posterior mean and Eq. (3) is the posterior variance-covariance matrix.

We consider two distinct model variants that formalize how the sensory-to-space transformation (Eq. 1) and Bayesian Integration (Eqns. 2 and 3) are implemented in the somatosensory processing hierarchy (**Figure 1B**).

In **model variant 1** (**Figure 1B**, top, **Figure 1C**, blue), Bayesian integration occurs *before* the sensory-to-space transformation. That is, the likelihood and the prior in Eqns.(2-3) are defined in sensory coordinates: The likelihood is specified as a Gaussian distribution with its mean $\boldsymbol{\mu}_{lik}$ defined by the involved rotation angles $(\theta_1, \ldots, \theta_n)$ and phalanx lengths $(L_1, \ldots, L_n)$. The likelihood variability Σ_{lik} is defined as a diagonal variance-covariance matrix specifying variance in sensory coordinates for joint angles $(\sigma_{\theta_1}^2, \cdots, \sigma_{\theta_n}^2)$ and phalanx lengths $(\sigma_{L_1}^2, \cdots, \sigma_{L_n}^2)$, and off-diagonal values set to zero (assuming uncorrelated noise). The prior is also defined in sensory coordinates and specified as Gaussian with mean $\boldsymbol{\mu}_{pr}$ and a variance-covariance matrix Σ_{pr}, allowing covariance between subsequent joint angles (i.e., between θ_1 and θ_2, θ_2 and θ_3).[38,39] The final step of this model variant transforms the sensory posteriors of the joint angles and segment lengths into proprioceptive localization behavior in space-based coordinates via Eq. (1). A coordinate transformation (CT) is therefore necessary. For each $\boldsymbol{l}_n$, as a linear approximation, we use the Jacobian J_n, derived from Eq. (1) by $J_n = \frac{\partial(x,y)}{\partial(\varphi,L)}$, to transform the

variance-covariance matrix of the sensory posterior (Σ_{sens}) to a variance-covariance matrix in spatial coordinates (Σ_{spat}), following:

$$\Sigma_{spat} = J_n * \Sigma_{sens} * J_n^T \quad (4)$$

In **model variant 2** (**Figure 1B**, bottom, **Figure 1C,** green), Bayesian integration occurs *after* the sensory-to-space transformation. The likelihood can be initially described by signals related to the individual joint angles and segment lengths of the finger (i.e., sensory coordinates). These sensory signals are first transformed into the Cartesian position of the finger $\boldsymbol{l}_n$ (via Eqns. 1 and 4), leading to a spatial likelihood with mean $\boldsymbol{\mu}_{lik}$ and covariance Σ_{lik} defined in Cartesian coordinates. The posterior spatial estimate of finger posture is defined as the product of this spatial likelihood and a spatial prior (via Eqns. 2-3), both represented in Cartesian coordinates.

Figure 1C illustrates the computational outcomes of each model in a Cartesian coordinate frame. The predicted posterior distribution of the PIP, DIP and FT positions are shown (variant 1 in blue; variant 2 in green) given their likelihood distributions for a simulated posture (solid gray line) and prior distribution (dashed gray line). As shown in **Figure 1D**, the inferred finger length (summed distance of segment lengths based on the posteriors of PIP, DIP and FT) in model variant 2 changes as a function of the spatial disparity between likelihood and prior (expressed as their Bhattacharya distance, see Eq. 7), i.e., as a function of posture (**Figure S1**).

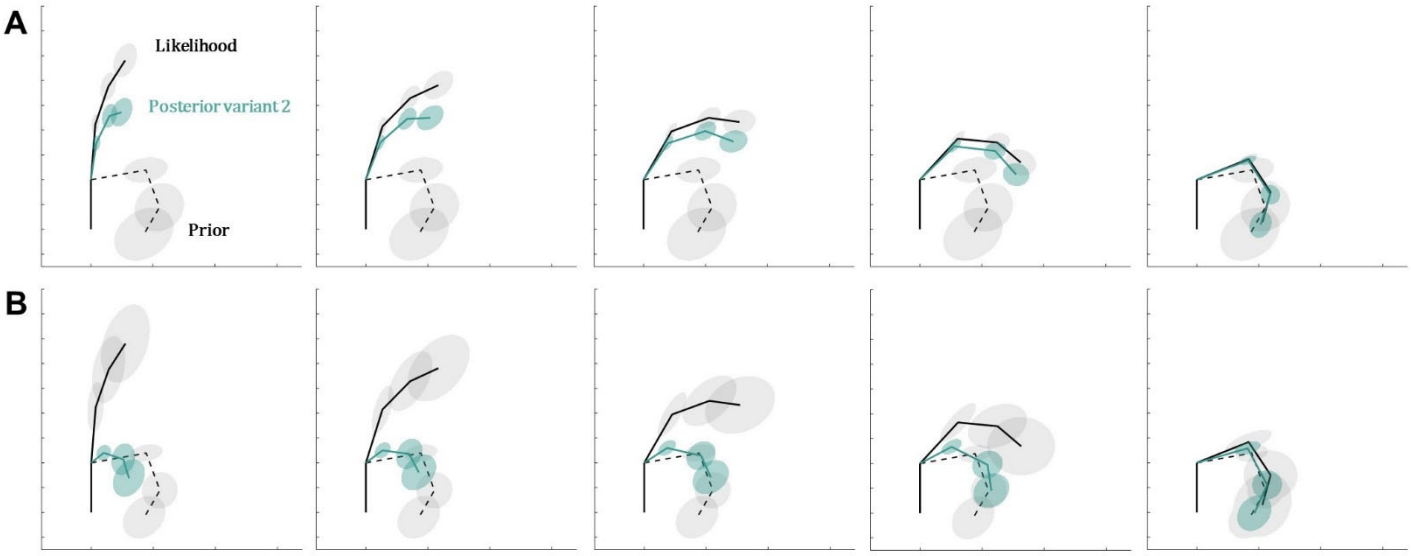

Figure S1. Model variant 2 predicts posture-dependent metric biases. A. Simulation of spatial posterior for variant 2 (green), with likelihood mean varying across six different postures (solid gray) and a fixed prior (dashed gray), suggests posture-dependent biases in perceived finger geometry. **B.** Note that these biases are also noise-dependent: in bottom panels, simulations are obtained using larger variances for likelihood and priors, with different outcomes in perceived finger configuration and geometry.

Participants

Twenty healthy volunteers (12 females) provided their informed consent and participated in the experiment. Participants were all right-handed (Edinburgh Handedness Inventory Short Form,[36] score > 75) and had a mean age of 21.55 ± 2.63 years. They all received course credits as compensation for participating in the experiment. The research was approved by the Ethics Committee of the Faculty of Social Sciences, Radboud University.

Position tracking and VR

We tracked the position of the index finger via infrared motion tracking (Optotrak Certus, Northern Digital Inc.), with a sampling rate of 100Hz. We used First Principles software to align coordinate systems of all position sensors into a global room-based coordinate system (i.e., registration). We used custom-made rigid bodies for each individual limb segment (forearm, hand dorsum, and the three phalanxes of the index finger) to track the position of the wrist, MC, PIP, DIP, and FT. Time stamps from the VR system were used to segment the continuous 3D signals into blocks corresponding to experimental conditions.

The VR environment was created with Unity. Participants wore an HTC Vive VR headset, while comfortably seated in a chair with their head supported by a chin rest. Images were presented with 1080*1200 pixel resolution to each eye at a 90 Hz refresh rate. The interocular distance was adjusted for each participant such that images were viewed with a field of view of 110˚. The VR space was aligned with Optotrak space using a calibration procedure supported by custom-made Python script. The alignment error was within 0.4 and 1.2 mm for all testing sessions.

Task and procedures

The experiment employed a VR finger mapping task to measure position estimates of the unseen left index finger joints (PIP, DIP) and FT at varying finger postures.

Participants were instructed to lay their left forearm on the table in front of them and grasp a cylinder with a power grip of their left hand (**Figure 2,** left). We used three cylindric volumes (height: 200 mm) having 20, 30, 40 mm diameter, each used to probe two different finger configurations, by holding the cylinder from its base, or from its body. Prior to the finger mapping task, participants completed a practice session to familiarize themselves with the virtual environment and task structure.

The VR environment (**Figure 2,** right) presented a dark three-dimensional space with horizon lines, and a realistic screen displaying written instructions. The actual locations of their left index MC and wrist were rendered as blue spheres (diameter 5 mm). This was done to capture perceptual biases related to finger configuration, rather than biases pertaining to the perceived position and configuration of the whole upper limb. Additionally, information on their total index finger length was conveyed via a yellow circumference, centered on the participant's left MC. The radius of the circle represented participant's finger length. This experimental choice was made in order to provide participants with unbiased information on the total length of their finger and rule out that possible finger length underestimation errors arise from spatial biases related to the perception of the virtual environment.

Participants were asked to hold a controller with their right hand, which included a virtual stick and pointer. On each trial, participants started with the virtual pointer at the start position (pointer held in the direction of the virtual monitor). The target of each trial (e.g., 'fingertip') was displayed on the virtual monitor. Participants were instructed to indicate with the virtual pointer the perceived location of e.g., their left index fingertip in space, and press a button to confirm the response. A green wheel

appeared on the pointer to indicate that the response was submitted. After each trial participants returned the right arm to the start position. Postures were probed across six experimental blocks, each involving a power grip probed by one of the cylinders. Each block contained 100 randomized trials, including 30 for PIP, DIP, and FT, and 5 trials for wrist and MC, for a total of 600 trials per participant. Trials were self-paced and each block lasted approximately 10 minutes.

Data preprocessing

For each subject, motion tracking data and behavioral responses were extracted in 3D coordinates and preprocessed using custom-made MATLAB code (R2022b). Two participants were excluded from the analysis as their data suggested they misunderstood the task instructions. We ascertained that participants kept their finger position constant during each block (variation < 1 mm across blocks and participants).

We aimed to analyze data in a 2D plane, i.e., the rotational plane of the finger. We thus applied geometrical rotations to the data of each block to align them on the z-axis, and reduce their dimensionality from 3D to 2D. Then, in order to subtract general biases in localization affecting all positions equally, we aligned the physical and perceived position of the MC to [0,0]. We then rotated each block of responses to align them on the physical MC-wrist axis, to align the perceived and physical hand dorsum and wrist.

For each distribution of estimates (i.e., for each subject, posture, and finger landmark), we aimed to exclude extreme ($p<.001$) multivariate outliers based on their statistical distance from the geometrical median of the distribution.[37] This led to the exclusion of on average 9.1% datapoints for each subject (in total: 891 datapoints out of 10800). **Figure S2** shows the data after alignment and outlier removal, with Cartesian positions normalized for total finger length (i.e., [x y]/total finger length).

We calculated the mean physical positions of wrist, MC, PIP, DIP and FT across blocks. These were used to extract fixed parameters for individual model fitting. In detail, we first computed the physical angles (in degrees) between the three vectors defined based on the relative positions of MC-PIP, PIP-DIP and DIP-FT. Then we calculated the length of each phalanx as the Euclidean distance (in mm) between MC-PIP, PIP-DIP, DIP-FT.

Model fitting and analyses

Model structure

The current section describes how we fit each model to the participants individual responses. As described in detail throughout the paper, we start by assuming that the postural state of a finger can be described as a set of interconnected segments having length $L_1, L_2,$ and L_3, and with rotation angles for the three joints θ_1, θ_2 and θ_3. Because of neural noise, these variables are defined as probability distributions having means and a variance-covariance structure. In the presence of noise, optimal behavior reduces to Bayesian decision making, where the perceived state of the finger (posteriors) corresponds to the integration of sensory measurements (likelihoods) and stored knowledge (priors). The goal of model fitting is therefore to find the set of parameters for the likelihood and prior that fit best to the data. Our procedure is as follows:

For the *likelihood*, we assumed that the sensory measurements ($\boldsymbol{\theta}$ and $\boldsymbol{L}$) were noisy but accurate. The parameter for the mean of each estimate was therefore fixed to its empirical value, i.e., the joint angle on that trial or the actual segment length. The parameter for the variance of each estimate was *free* to vary within realistic constraints. To reduce the number of free parameters, we assumed that likelihood variance over joint angle is similar across joints, and variance over phalanx length is similar across phalanges. We also assumed that the noise in the sensory measurements is uncorrelated.

Off-diagonal values for likelihood covariances were therefore fixed at zero. In total, the fitting for the likelihood had six fixed parameters and two free parameters.

For the *prior*, we had different assumptions for signals encoding joint angles and phalanx length. The parameter for the prior means over joint angles was *free* to vary within realistic constraints. In contrast, we assumed accurate priors over phalanx length; we thus fixed the parameter for the means of these priors to their empirical values. The rationale behind these assumptions lies in the biomechanical features of the finger: while joint angles continuously vary, the length of each phalanx is stable in the short-term. It follows that sensory signals on phalanx lengths reflect the actual finger geometry, leading to an accurate measurement distribution. The prior distribution of length is accurate as well, since it is learnt over sensory feedback gathered during previous sensorimotor interactions with the environment. Regarding the prior variance-covariance, we let the variance of each estimate free to vary within realistic constraints. We set the correlation between two sets of joint-pairs as free to vary, given known covariances between them (see[38,39]). All other off-diagonal values were set at 0. In total, the fitting for the prior had three fixed parameters and eleven free parameters.

The full model therefore had 22 parameters (13 free, **Table S1**) that were inputted into the functions described by Eqns. (1-4) via custom-made MATLAB code, following the computational steps of model variant 1 or model variant 2. It is critical to note that the fitting for each model variant had the same free and fixed parameters.

Table S1. Hard boundaries for model parameter search space

	Lik. variance		Prior mean			Prior variance-covariance							
	$\sigma_{\theta,lik}$ deg	$\sigma_{L,lik}$ mm	$\theta_{1,pri}$ deg	$\theta_{2,pri}$ deg	$\theta_{3,pri}$ deg	$\sigma_{\theta_1,pri}$ deg	$\sigma_{\theta_2,pri}$ deg	$\sigma_{\theta_3,pri}$ deg	$\rho_{\theta_{1,2},pri}$	$\rho_{\theta_{2,3},pri}$	$\sigma_{L_1,pri}$ mm	$\sigma_{L_2,pri}$ mm	$\sigma_{L_3,pri}$ mm
Lower bound	0.1	0.1	-20	-10	-10	0.1	0.1	0.1	-0.8	-0.8	0.1	0.1	0.1
Upper bound	35	50	90	100	70	45	45	45	0.8	0.8	50	50	50

Model fitting and evaluation

To estimate best fitting parameters for each subject and model variant, we maximized the probability of the data (observed behavioral estimates expressed in spatial coordinates), given a range of initial parameters and model variant. We applied Maximum Likelihood Estimation (MLE) to maximize the log-likelihood, with log-likelihood based on a 2D Gaussian function and calculated as:

$$LL = \mathrm{p}(\boldsymbol{obs}|\boldsymbol{\mu}, \Sigma) = \log(\sum_{i=1}^{N} 2\pi^{-\frac{k}{2}} |\Sigma|^{-\frac{1}{2}} e^{-\frac{1}{2}(\boldsymbol{obs}_i - \boldsymbol{\mu})\Sigma^{-1}(\boldsymbol{obs}_i - \boldsymbol{\mu})}) \quad (5)$$

in which N is the number of observations; k is the number of free parameters in the model; **obs** represent observed localization judgements (expressed in 2D spatial coordinates), relative to MC position (0,0); **μ** and Σ are model's posterior mean and covariance (expressed in 2D spatial coordinates), given each initial set of free parameters.

Optimization of the -LL was done using *fmincon* (MATLAB) as done previously.[21,40] For every model variant and participant, we computed 100 fits using random parameter initializations. We then selected the best fit as the one associated with minimum -LL (**Table S2**).

For each best fit we then calculated the BIC (Bayesian Information Criterion). This expresses the maximized log-likelihood (LL) as a function of the number of observations (N) and free parameters (k).

$$BIC = -2 * LL + log(N) * k \quad (6)$$

We compared BIC distributions using paired t-test. Lower BICs indicate better fits.

As an indication of the quality of the model fits we computed the R^2 for each subject. This was calculated by subtracting from 1 the ratio between the sum of squared distances between predicted and observed mean estimates and the sum of squared distances between observed mean estimates and their grand mean over postures.

If model variant 2 well approximates behavioral estimates, we would expect that the observed finger length estimation bias (estimated finger length – actual finger length) / actual finger length *100) varies as a function of the distance between the prior and the likelihood, as shown by model simulations (**Figure 1D**). This distance was quantified as Bhattacharya distance (a variation of the Mahalanobis distance), computed based on the fitted likelihood and prior expressed in Cartesian coordinates:

$$\Delta_{lik-pr} = \sum_{i=1}^{n} -\frac{1}{2}\left(\boldsymbol{\mu}_{lik} - \boldsymbol{\mu}_{pr}\right)^T \left(\frac{\Sigma_{lik} + \Sigma_{pr}}{2}\right)^{-1} \left(\boldsymbol{\mu}_{lik} - \boldsymbol{\mu}_{pr}\right) \quad (7)$$

Table S2. Fitted parameter values and fit outcome for each subject and model variant

Subject	Variant	Likelihood		Prior											Fit outcomes		
		$\sigma_{\theta,lik}$	$\sigma_{L,lik}$	$\theta_{1,pri}$	$\theta_{2,pri}$	$\theta_{3,pri}$	$\sigma_{\theta_1,pri}$	$\sigma_{\theta_2,pri}$	$\sigma_{\theta_3,pri}$	$\sigma_{L_1,pri}$	$\sigma_{L_2,pri}$	$\sigma_{L_3,pri}$	$\rho_{\theta_{1,2},pri}$	$\rho_{\theta_{2,3},pri}$	-LL	BIC	R^2
1	1	9.81	50.00	-20.00	100.00	-10.00	16.75	11.95	23.91	12.28	6.14	4.89	0.50	0.50	3744.34	7570.47	0.62
	2	8.91	10.39	-20.00	100.00	70.00	12.48	24.95	14.13	17.14	8.57	9.53	-0.36	0.80	3660.64	7403.08	0.69
2	1	23.24	50.00	21.60	100.00	17.36	12.45	6.22	12.45	14.43	7.21	3.61	0.12	0.50	3849.08	7779.94	0.23
	2	7.95	18.43	68.34	84.50	35.23	13.93	11.43	17.00	10.13	12.72	19.72	-0.80	-0.80	3620.36	7322.52	0.54
3	1	21.53	50.00	90.00	99.69	-10.00	28.42	15.92	10.59	21.87	10.93	5.47	-0.50	0.50	4361.78	8805.36	0.27
	2	16.61	20.59	90.00	60.71	-10.00	12.19	18.18	36.36	19.58	21.13	15.63	-0.80	0.33	4144.62	8371.04	0.68
4	1	35.00	38.23	-20.00	-10.00	70.00	24.81	34.43	20.50	23.99	18.49	9.84	-0.50	0.50	4579.12	9240.03	-0.04
	2	35.00	50.00	-20.00	0.28	70.00	27.17	45.00	45.00	22.26	15.51	7.75	-0.80	-0.56	4518.88	9119.54	0.01
5	1	11.05	50.00	90.00	100.00	-10.00	40.42	20.21	17.61	14.04	7.02	14.04	-0.50	0.50	3845.46	7772.70	0.45
	2	12.23	10.51	90.00	80.26	0.11	15.92	11.08	21.20	17.01	17.47	34.93	-0.80	0.80	3695.19	7472.18	0.68
6	1	24.95	50.00	77.80	70.34	-10.00	26.01	16.79	33.35	17.22	8.61	4.31	-0.50	0.50	4148.18	8378.15	0.49
	2	15.80	23.61	84.40	30.10	-10.00	26.78	45.00	22.50	12.76	8.83	17.66	-0.80	-0.43	4010.55	8102.88	0.68
7	1	35.00	50.00	7.15	28.55	19.60	5.43	7.79	11.97	29.90	14.95	7.48	-0.50	-0.50	3937.27	7956.34	-0.24
	2	35.00	50.00	6.92	30.14	12.73	5.99	11.98	23.96	30.21	15.11	7.55	-0.80	-0.69	3917.26	7916.31	-0.26
9	1	35.00	50.00	7.36	64.54	70.00	18.79	23.69	32.01	16.61	8.30	4.15	-0.50	0.50	4278.56	8638.90	0.61
	2	35.00	16.74	6.71	72.83	-10.00	21.37	42.75	21.37	23.19	11.59	5.80	-0.80	-0.69	4244.51	8570.80	0.54
10	1	21.12	50.00	-20.00	100.00	70.00	31.17	45.00	22.50	34.06	20.97	10.49	0.50	-0.50	4576.86	9235.51	0.15
	2	21.75	50.00	-20.00	86.59	-3.63	24.47	36.50	45.00	32.01	19.08	9.54	-0.80	-0.80	4480.15	9042.09	0.25
12	1	35.00	50.00	20.71	79.20	-10.00	9.25	6.03	7.97	23.72	11.86	5.93	-0.50	-0.50	4182.04	8445.87	0.34
	2	10.23	48.25	46.02	-10.00	69.93	10.99	21.97	10.99	16.04	8.02	13.15	-0.71	-0.74	3884.74	7851.28	0.76
13	1	17.00	50.00	-1.41	100.00	70.00	20.31	10.15	19.35	19.78	9.89	4.95	-0.50	-0.50	4203.70	8489.19	0.09
	2	11.33	14.61	90.00	100.00	70.00	19.83	39.65	24.95	30.59	15.30	7.65	-0.80	-0.12	4106.63	8295.05	0.37
14	1	35.00	50.00	-19.60	39.73	70.00	13.56	16.07	8.03	17.40	8.70	17.40	0.50	-0.50	4147.30	8376.39	-0.05
	2	17.57	13.81	-20.00	17.38	-10.00	11.81	23.62	22.78	31.26	15.63	7.81	-0.47	-0.80	3948.82	7979.43	0.48
15	1	30.40	50.00	-20.00	100.00	56.74	45.00	45.00	22.50	11.78	12.39	6.20	0.50	-0.50	4255.63	8593.04	0.45
	2	33.54	19.06	-20.00	95.92	41.66	45.00	22.50	43.66	15.98	7.99	4.00	-0.05	-0.80	4216.25	8514.28	0.44
16	1	20.45	50.00	-12.64	100.00	-10.00	45.00	22.50	22.12	14.28	7.14	3.57	0.28	0.50	4132.81	8347.40	0.53
	2	27.08	12.26	7.02	100.00	16.59	26.12	32.65	45.00	30.22	15.11	7.55	0.80	-0.80	4074.06	8229.91	0.54
17	1	21.46	50.00	12.10	100.00	45.95	11.11	5.56	4.98	20.90	10.45	5.23	0.50	-0.50	4125.69	8333.17	-0.48
	2	8.28	17.65	90.00	64.13	6.47	15.88	31.75	45.00	20.01	38.03	50.00	-0.80	-0.80	3990.16	8062.11	0.24
18	1	18.61	50.00	23.69	100.00	70.00	21.14	10.57	20.51	19.45	9.72	6.80	0.43	-0.50	4125.59	8332.97	-0.39
	2	9.76	19.96	90.00	54.44	9.35	16.76	33.52	45.00	20.27	35.19	50.00	-0.80	-0.80	3970.59	8022.97	0.39
19	1	35.00	50.00	-16.11	100.00	55.78	20.53	10.26	17.81	24.58	12.29	18.59	-0.50	-0.50	4356.71	8795.20	-0.01
	2	22.62	50.00	-20.00	100.00	38.27	22.95	35.44	45.00	23.00	11.50	23.00	0.80	-0.80	4281.88	8645.54	-0.12
20	1	8.32	50.00	19.89	-10.00	20.67	5.96	5.06	3.62	32.28	27.05	13.53	-0.50	-0.50	4105.16	8292.11	-4.10
	2	8.46	18.18	7.25	-10.00	24.21	5.91	11.83	21.31	32.47	50.00	25.00	-0.80	-0.80	3803.94	7689.67	-0.41

Ruling out response truncation

During the task, participants in VR could see the position of their MC and a yellow circumference centered on the MC. The circumference's radius represented the total length of participant's index finger when stretched (**Figure 2**). This experimental choice was made in order to provide participants with unbiased information of the size of their finger, and rule out that possible finger length underestimation errors arise from spatial biases related to the perception of the virtual environment. However, it is possible that providing this information would lead to a truncation of response distributions for the fingertip, especially in case participant's fingertips happened to be very close to or overlapping with the circumference (i.e., extended finger posture). We took two approaches to rule out this possibility.

First, if our results were due to truncation of the fingertip response distribution, we would have expected to observe underestimation of the tip phalanx (i.e., distance between DIP and FT), and not of the other segments, i.e., base phalanx (MC-PIP) and middle phalanx (PIP-DIP). Instead, as it is visible in **Figure S2,** spatial biases affect not only FT, but also DIP and PIP estimation responses. Specifically, segment length misestimation across postures and participants was on average -8.65% (± SEM 5.06) for the base segment, -24.68% (± 6.28) for the middle segment, and 1.26% (± 7.82) for the tip segment. One-tailed t-test against zero showed that underestimation is significant for the middle segment ($t(17) = -3.93$, $p = .001$), marginally significant for the base segment ($t(17) = -1.71$, $p = .053$ and not significant for the tip segment ($t(17) = 0.16$, $p = .563$). These spatial biases lead to an average total misestimation across segments, postures and participants of -19.51 (± 4.42) with $t(17) = -4.41$, $p < .001$. This pattern of results—and specifically, the lack of underestimation for the tip phalanx—would not be expected our results were simply due to response truncation.

Second, if our results were solely due to the avoidance of the imposed boundary, we would expect that participants truncated their response distributions at that boundary. In contrast, we consistently observed estimates beyond this boundary. In the polar plots of **Figure S3**, the radius of circumferences represents the distance from MC and FT when the finger is extended, i.e., total finger length. The black segments represent the six tested postures, each associated with a different color. Response distributions for the FT are colored accordingly. As a first observation, fingertip position for most postures and participants did not lie close to the circumference. The task indeed probed different power grips, requiring different degrees of finger flexion. This minimizes the possibility that responses were truncated, as response targets did not lie on the boundary. This is visible also in histograms, in which the solid line represents the normalized distance from MC to FT (physical distance / total finger length), and the dashed line the circumference radius normalized to one. Frequency distributions represent different blocks (i.e., postures), colored coherently with polar plots. If truncation occurred, we would have expected fingertip estimation responses to cluster *within* the circle. Rather, in some cases (e.g., in subjects 4, 6, 14), responses cross the circle boundary, coherently with non-truncated distributions.

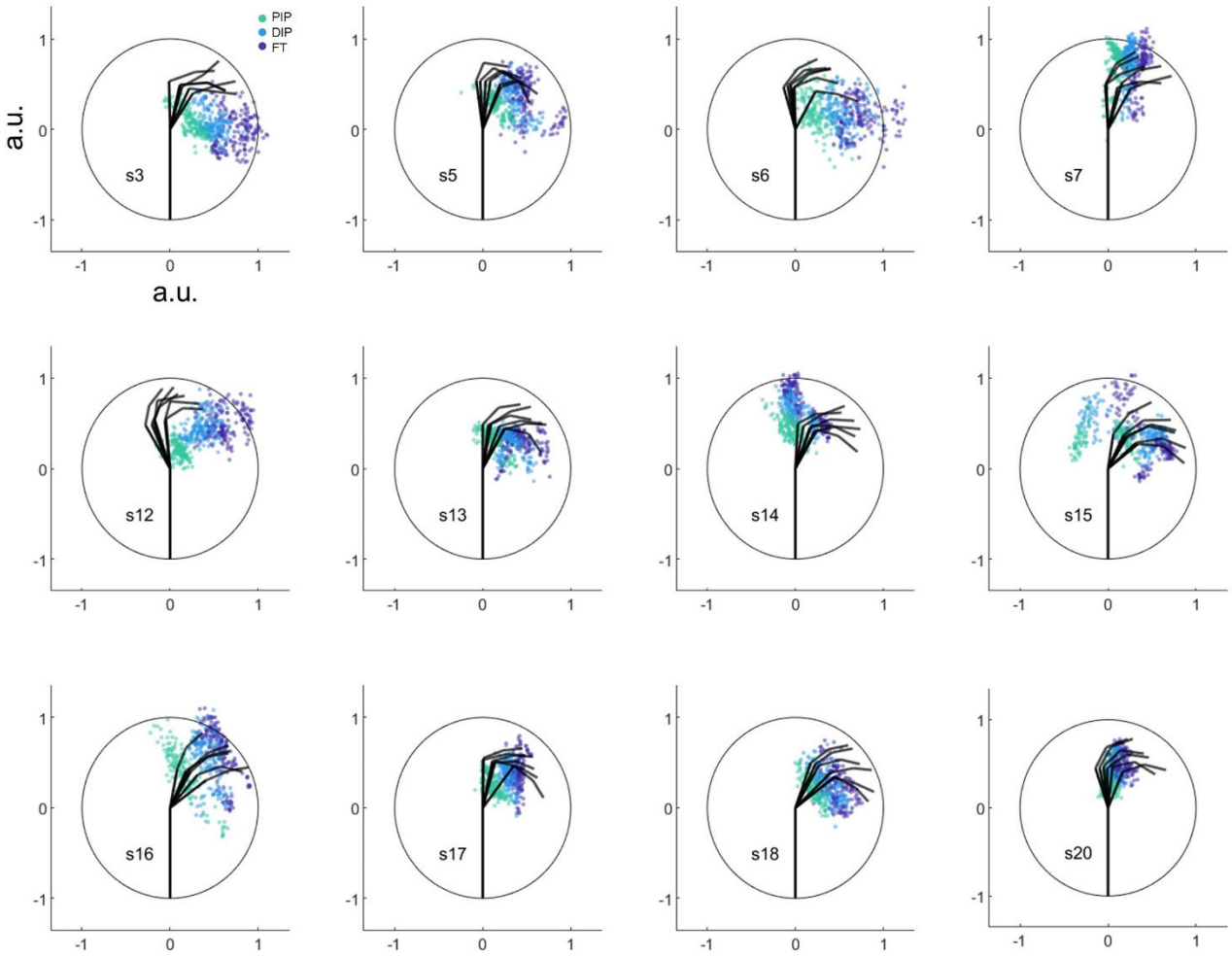

Figure S2. Examples of preprocessed data. Each polar plot shows the normalized circumference (i.e., rendered yellow circle) centered on participant's MC, along with the six tested postures (black segments), and behavioral responses for PIP (green), DIP (blue), FT (purple).

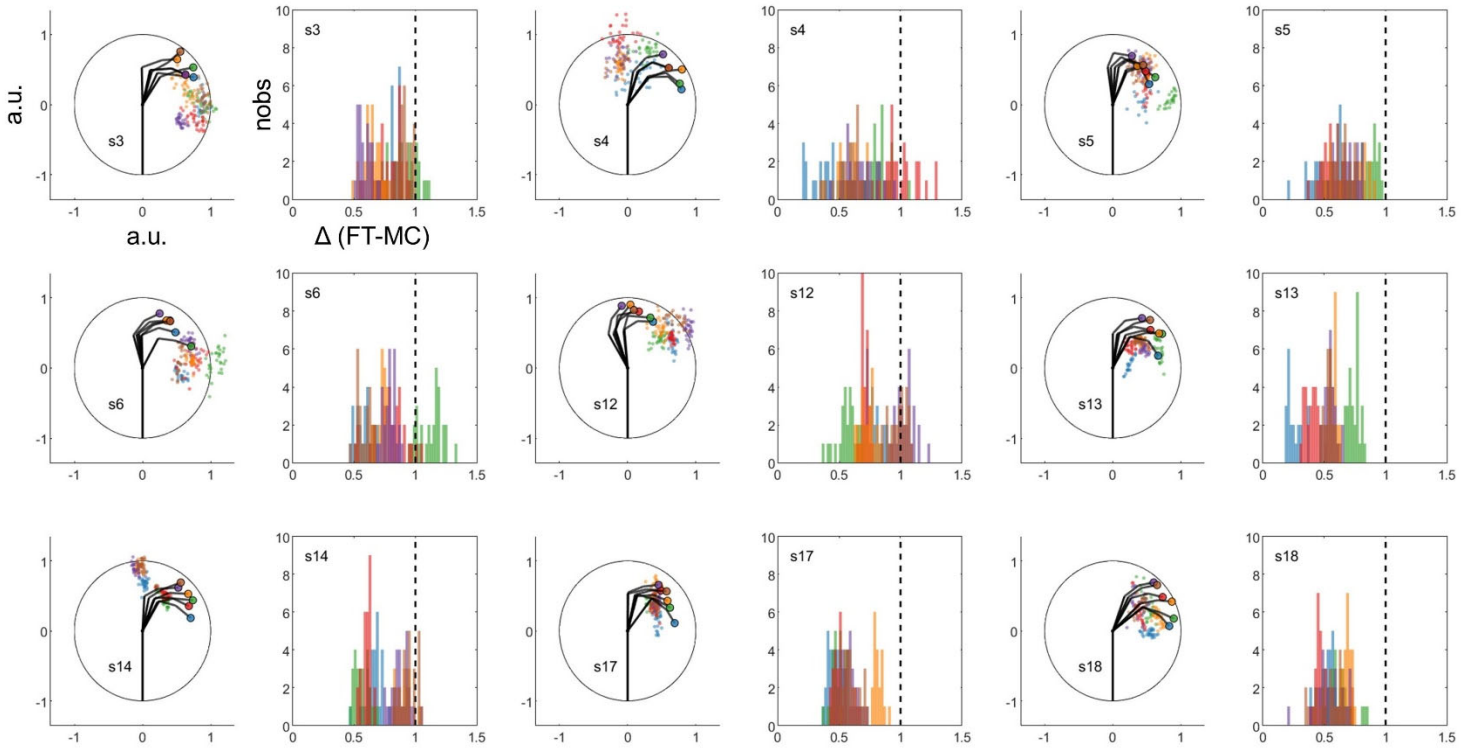

Figure S3. Ruling out response truncation. Each polar plot shows the normalized circumference (i.e., rendered yellow circle) centered on participant's MC, along with the six tested postures (black segments). Fingertip localization responses for a subject (i.e., Cartesian positions normalized on total finger length) are represented as small dots; each color represents a posture. Accordingly, real fingertip positions across postures are plotted as big colored dots. The same colors are used to represent frequency distributions of the estimated distance between MC and FT. Black dashed line represents total finger length.